Molecular Cell, Vol. 20, 867–879, December 22, 2005, Copyright ©2005 by Elsevier Inc. DOI 10.1016/j.molcel.2005.11.008

Localization of the Coactivator Cdh1 and the Cullin Subunit Apc2 in a Cryo-Electron Microscopy Model of Vertebrate APC/C

Prakash Dube,[1,4] Franz Herzog,[2,4] Christian Gieffers,[2,4,5] Bjoern Sander,[1] Dietmar Riedel,[1] Shirley A. Müller,[3] Andreas Engel,[3] Jan-Michael Peters,[2,*] and Holger Stark[1,*]

[1] Max-Planck-Institute for Biophysical Chemistry
Am Fassberg 11
37077 Goettingen
Germany

[2] Research Institute of Molecular Pathology
Dr. Bohr-Gasse 7
1030 Vienna
Austria

[3] Maurice E. Müller Institute
Biozentrum
University of Basel
CH-4056 Basel
Switzerland

Summary

The anaphase-promoting complex/cyclosome (APC/C) is a ubiquitin ligase with essential functions in mitosis, meiosis, and G1 phase of the cell cycle. APC/C recognizes substrates via coactivator proteins such as Cdh1, and bound substrates are ubiquitinated by E2 enzymes that interact with a hetero-dimer of the RING subunit Apc11 and the cullin Apc2. We have obtained three-dimensional (3D) models of human and *Xenopus* APC/C by angular reconstitution and random conical tilt (RCT) analyses of negatively stained cryo-electron microscopy (cryo-EM) preparations, have determined the masses of these particles by scanning transmission electron microscopy (STEM), and have mapped the locations of Cdh1 and Apc2. These proteins are located on the same side of the asymmetric APC/C, implying that this is where substrates are ubiquitinated. We have further identified a large flexible domain in APC/C that adopts a different orientation upon Cdh1 binding. Cdh1 may thus activate APC/C both by recruiting substrates and by inducing conformational changes.

Introduction

The APC/C is a ubiquitin ligase (E3 enzyme) that has important functions in mitosis, meiosis, G1 phase of the cell cycle, and in postmitotic differentiated cells (reviewed in Harper et al. [2002] and Peters [2002]). In all these situations, APC/C is first activated by transient association with one of several coactivator proteins, called Cdc20, Cdh1, and Ama1, and then collaborates with the ubiquitin conjugating (E2) enzymes Ubc4 and UbcH10 to assemble ubiquitin chains on substrate proteins. This modification targets the substrates for degradation by the 26S proteasome. In mitosis, APC/C is essential for the separation of sister chromatids in anaphase and for subsequent exit from mitosis. APC/C initiates these events by ubiquitinating mitotic cyclins, the activating subunits of cyclin-dependent kinase 1 (Cdk1), and by ubiquitinating securin, an inhibitor of the protease separase that dissolves sister chromatid cohesion by cleaving cohesin complexes. Although these processes are essential for cell proliferation in presumably all eukaryotes, it is still poorly understood how APC/C assembles ubiquitin chains on its substrates.

Human APC/C is composed of at least 12 different proteins that are constitutively present in the complex. Two of these, called Apc2 and Apc11, contain cullin and RING finger domains, respectively (Yu et al., 1998; Zachariae et al., 1998b). RING finger domains are also found in numerous other ubiquitin ligases where they have been shown to interact with E2 enzymes (Lorick et al., 1999; Zheng et al., 2000), whereas cullin proteins are subunits found in a family of ubiquitin ligases called Skp1-Cdc53/Cul1-F box (SCF) complexes (reviewed in Petroski and Deshaies [2005]). Cullins are thought to function as scaffold proteins because their C-terminal cullin domain binds to a RING finger subunit, whereas their N terminus recruits one of several substrate binding proteins, typically indirectly via interaction with an adaptor protein. One type of SCF complex can interact with different substrate binding proteins; for example SCF1, which contains the cullin subunit Cul1, can bind to numerous different F box proteins, resulting in a modular system that is able to ubiquitinate different substrates. It is not known by which mechanism ubiquitin is transferred from E2 enzymes to lysine residues on the substrates, but it is generally assumed that RING finger E3s function as platforms that bring ubiquitin-charged E2s and substrates into close proximity without directly participating in the catalysis of the ubiquitination reaction (reviewed in Passmore and Barford [2004]).

Similar to the situation in SCF complexes, the cullin domain of Apc2 binds to the RING finger subunit Apc11, which is able to interact with Ubc4 (Gmachl et al., 2000; Leverson et al., 2000; Tang et al., 2001). APC/C can also be regulated in a modular fashion, although to a smaller extent than SCF, through association with the coactivator proteins Cdc20, Cdh1, and Ama1. Like some F box subunits of SCF, these proteins contain a WD40 domain that is predicted to form a propeller-like structure. In the case of Cdh1, it has been shown that this WD40 domain binds directly to sequence elements in APC/C substrates that are required for their ubiquitination called destruction (D) and KEN boxes (Kraft et al., 2005). Cdh1 and substrates then form a ternary complex with APC/C by binding of Cdh1 to the tetratrico peptide repeat (TPR) subunit Cdc27 (Burton et al., 2005; Kraft et al., 2005; Passmore et al., 2005).

For a more detailed understanding of how substrates are ubiquitinated by APC/C and how this process is controlled, it will be important to obtain insight into the structure of the APC/C, but so far only the crystal

*Correspondence: peters@imp.univie.ac.at (J.-M.P.); hstark1@gwdg.de (H.S.)

[4] These authors contributed equally to this work.

[5] Present address: AFFIRIS GmbH, Viehmarktgasse 2a, 1030 Vienna, Austria.

structures of the small APC/C subunit Doc1 and of a fragment of Apc2 are known (Au et al., 2002; Wendt et al., 2001; Zheng et al., 2002). Because crystallization of the whole APC/C has not yet been possible, we have begun to use cryo-EM to analyze the structure of APC/C (Gieffers et al., 2001). Here, we present a refined model of APC/C purified from human cells and from *Xenopus laevis* eggs, which we obtained by cryo-negative staining, angular reconstitution, and RCT EM analyses. We have used STEM to determine the molecular mass of human and *Xenopus* APC/C, and we provide evidence that several of APC/C's TPR subunits are present in supra-stoichiometric amounts relative to other subunits. We have used EM techniques in conjunction with biochemical reconstitution of APC/C bound to Cdh1 (APC/C^{Cdh1}) and antibody labeling to map the locations of the coactivator Cdh1 and the cullin domain of Apc2. Finally, we have identified a highly flexible domain in human APC/C. A conformational rearrangement of the same structural domain has also been observed upon binding of Cdh1 to *Xenopus* APC/C, suggesting that the inherent flexibility of APC/C may be important for its regulation or function.

Results

Purification of APC/C for EM Analyses

To analyze APC/C's structure, we previously purified complexes from HeLa cells in the Peters lab and shipped them overnight on ice to the Stark lab for EM preparation (Gieffers et al., 2001). In EM, we observed numerous V shaped particles, which we assume represent APC/C, and whose images we analyzed by angular reconstitution for 3D structure determination. However, we also saw smaller particles of irregular shape that presumably represent disintegrated forms of APC/C. We therefore first improved the quality of our samples by optimizing the APC/C purification protocol. We noticed that Apc2 and Apc11 selectively dissociated from the rest of the complex when APC/C was exposed to buffers with neutral or slightly acidic pH values and increased ionic strength (Vodermaier et al., 2003). Similarly, we observed in negative staining EM experiments that exposures to low pH values, treatment with 500 mM NaCl, and prolonged storage of APC/C increased the abundance of disintegrated particles (data not shown). In contrast, the percentage of apparently intact particles was considerably increased when APC/C was purified in a buffer with a pH of 7.6 that contained only 150 mM NaCl, and the EM preparation was done immediately afterward. We therefore isolated APC/C under these conditions from logarithmically proliferating HeLa cells by Cdc27 antibody affinity chromatography and prepared negatively stained cryo-specimens from fresh samples by the double carbon foil sandwich technique (Golas et al., 2003). The purity of all samples was analyzed by SDS-PAGE and silver staining (Figure 1A).

The Structure of Human and *Xenopus* APC/C Determined by Angular Reconstitution and RCT Analysis

The structure of human APC/C was determined by angular reconstitution from ~30,000 cryo-negative stain images. A typical raw image is shown in Figure 1B. The image analysis revealed very good agreement of raw images, corresponding class averages, and reprojections computed from the 3D map (Figures 1C–1F) showing the internal consistency of the image analysis and 3D structure determination. A comparison between the new (Figures 1E and 2A) and our previously obtained 3D model of human APC/C (Gieffers et al., 2001) revealed both similarities and differences. In both models, APC/C has an asymmetric shape with one convexly curved side, the "back," and the opposite side, the "front side," being concavely curved. This explains why APC/C appears as a V shaped particle in projection images. Furthermore, in both the present and the previous models, APC/C is composed of an outer proteinaceous wall that encloses an inner cavity (best seen in cross-sections; Figure 2B) and has a prominent "head"-like structure at one end. However, in the old model, the inner cavity is connected with the exterior by a large opening on the front side, whereas in the new model, this opening is largely obscured by additional protein mass.

To address whether the new model represents a more realistic view of APC/C, we purified APC/C from a different vertebrate species with highly homologous protein composition, the clawed frog *Xenopus laevis*, and independently subjected it to the same negative staining 3D cryo-EM analysis as human APC/C. The 3D model of APC/C purified from *Xenopus* interphase egg extracts (Figure 1A) turned out to be very similar to the model obtained for human APC/C (Figure 2A). In particular, in both models, a distinct protein mass is seen in the center of the front side, where an opening was observed in the older model of human APC/C. We believe that this opening arose from a previously unknown biochemical disintegration effect that may have been caused by storage and transport of APC/C in buffers with suboptimal pH and ionic strength conditions. For example, it is possible that Apc2 and Apc11 dissociated from APC/C particles under these conditions and that this process resulted in a decrease in protein mass on the front side of APC/C where these proteins normally appear to be located (see below).

Architecture of Human and *Xenopus* APC/C and Determination of Handedness

The new models of APC/C reveal several peculiar structural features such as a relatively flat platform (~180 by 200 Å in size) with a surrounding wall that encloses the central cavity together with an "arc lamp"-like structural element (~226 Å from top to bottom, Figure 2A). Between the top of the arc lamp and the platform, a central density element is located that gives the complex a more compact appearance and prevents the view inside where the large central cavity is present. The pattern of contacts between the central density, the platform, and the arc lamp is different in human and *Xenopus* APC/C. This pattern also changes upon binding of Cdh1 to *Xenopus* APC/C (see below), indicating that the contacts have an important functional role. These changes are accompanied by structural rearrangements of the platform wall, especially in the region that is in contact with the central density.

Structure determination of APC/C is not a trivial task due to the presence of a pseudo mirror symmetry (V like shapes) in projection images (Figure 1) and a certain

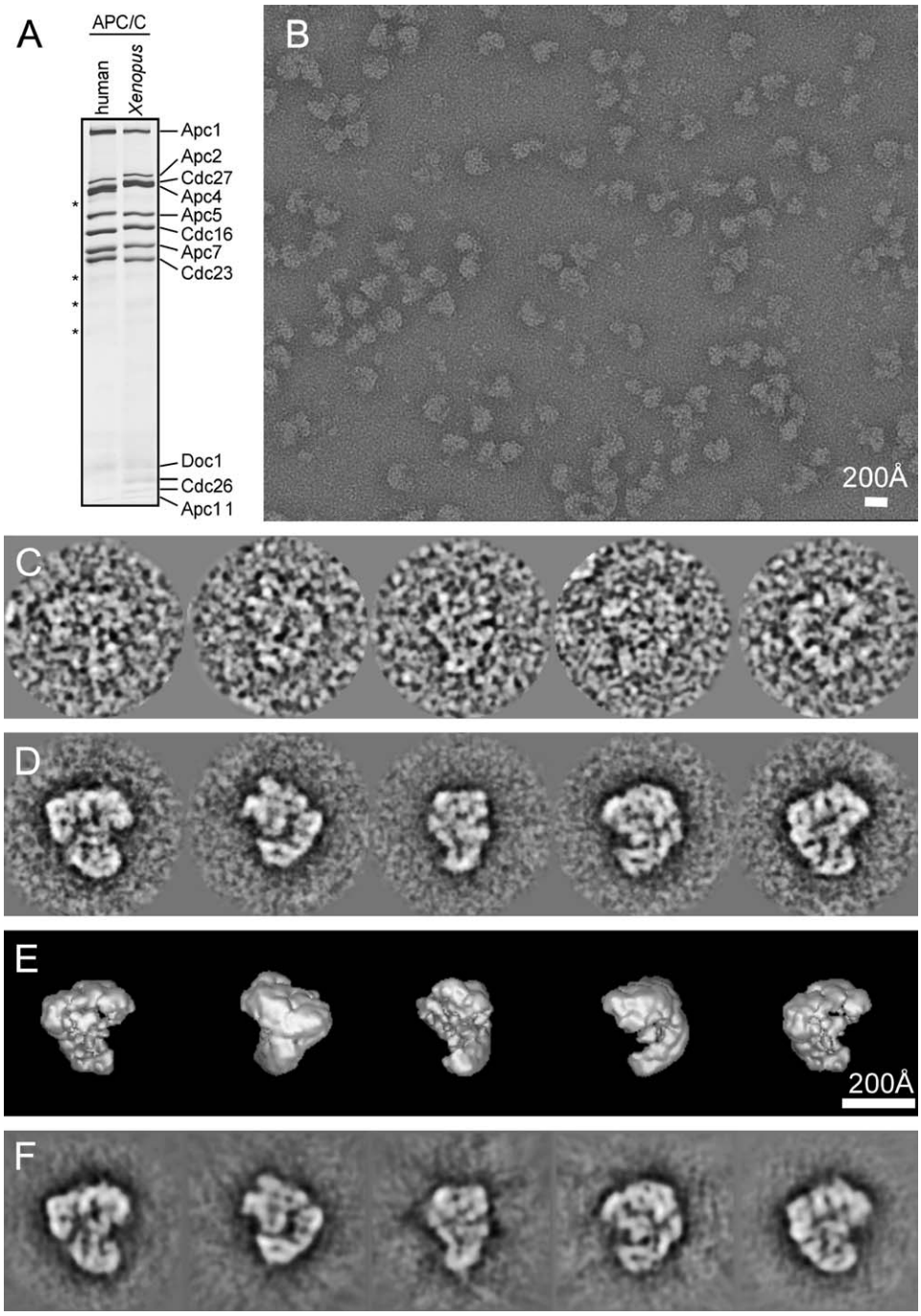

Figure 1. Purification and EM of APC/C

(A) APC/C immunopurified from logarithmically proliferating HeLa cells and *Xenopus laevis* interphase eggs was separated on SDS-PAGE, and subunits were detected by silver staining. Asterisks (*) indicate degradation products of Cdc27 and Apc7.

(B) EM raw images of human APC/C prepared by the double carbon foil sandwich technique.

(C) Selected raw images of human APC/C complexes.

(D) Corresponding class averages of the raw images shown in (C). The final class averages were obtained by alignment, multivariate statistical analysis, and classification.

(E) Surface views of the computed APC/C 3D structure shown in the orientations that corresponds to the views shown in (D).

(F) Reprojections of the APC/C 3D structure in angular direction determined for the views in (D).

degree of sample heterogeneity (described below). It is likely that the algorithms used to determine the angular orientation of V shaped images fail in discriminating correctly between mirror views. As a result, our initial 3D reconstructions yielded a pseudo symmetrical 3D model (data not shown). However, by careful selection of the views used to compute the 3D model, we were able to avoid the bias introduced by the dominant V shaped

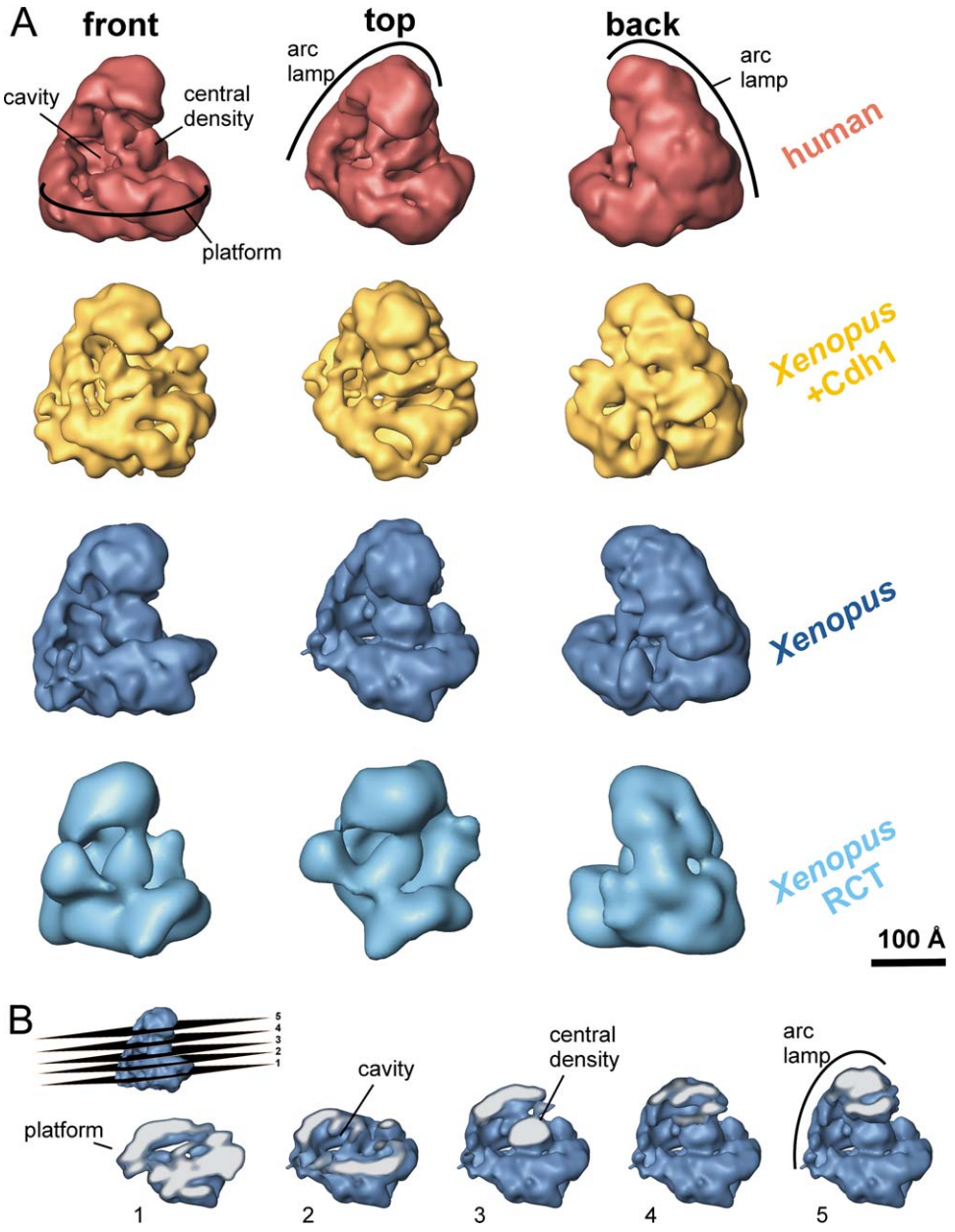

Figure 2. Three-Dimensional Structure of Human and *Xenopus* APC/C

(A) Surface views of the human APC/C, *Xenopus* APC/C^{Cdh1}, and *Xenopus* APC/C structures determined by angular reconstitution and of the *Xenopus* APC/C structure determined by the RCT technique. The main features are indicated on the human APC/C structure: the platform with an outer wall and the arc lamp structure enclose a central cavity. The central density connects the arc lamp domain and the platform. The dimensions are ~226 Å from top to bottom and ~200 × 180 Å for the size of the platform. The RCT structure shows the same overall structural elements as the others and additionally reveals the handedness.

(B) Sections through the *Xenopus* APC/C reconstruction as shown from bottom to top. The view corresponds to the front view shown in (A) for the *Xenopus* APC/C structure determined by angular reconstitution. The slices are indicated and numbered one to five in the small inset.

images. To further test the validity of the resulting 3D model, we performed an RCT experiment (Radermacher et al. 1987). The advantage of the RCT technique is that two of the three angular parameters needed for 3D reconstruction can be directly measured and the handedness of the structure is preserved. Therefore, the RCT structure of *Xenopus* APC/C was extremely helpful to independently corroborate the correctness of the 3D structure determined by angular reconstitution. In all, ~2000 tilted pairs of *Xenopus* APC/C images were recorded to compute the RCT 3D reconstruction at 40 Å resolution. The correctness of image alignment was improved by the use of a CCD detector instead of film, leading to an about 2-fold increased image signal in the resolution range of typical RCT reconstructions (Sander et al., 2005). Importantly, no pseudo symmetry appeared in the RCT reconstruction of *Xenopus* APC/C with an overall shape very similar to the higher resolution structures of *Xenopus* and human APC/C determined by angular reconstitution (Figure 2A).

A

Particles	human APC/C	X.I. APC/C
Molecular mass	1378 kDa	1533 kDa
Standard deviation	±213 kDa	±206 kDa
Sample size	n = 448	n = 831
Overall uncertainity	70 kDa	77 kDa

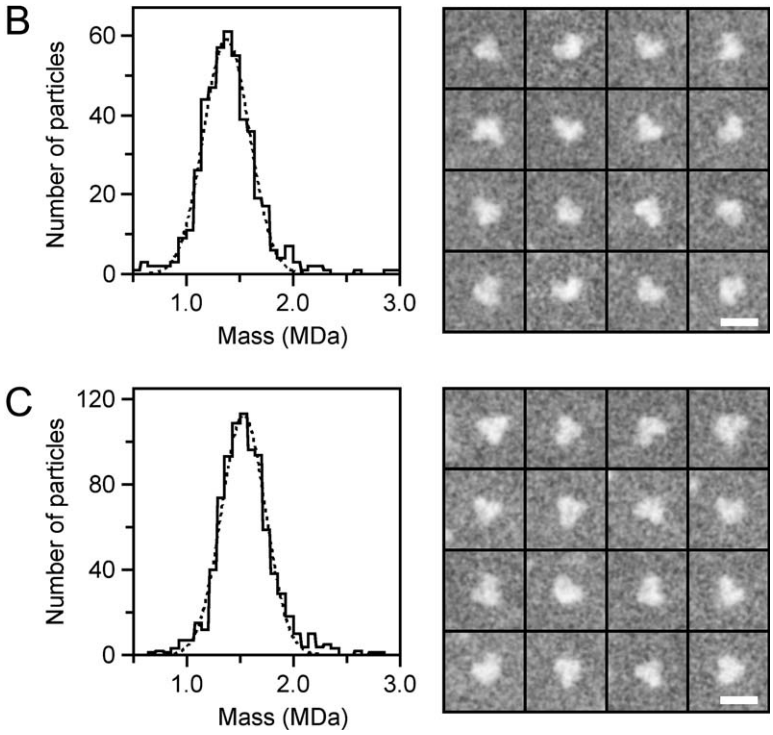

Figure 3. Mass Measurement of APC/C by STEM

(A) Summary of the STEM mass analysis of human and *Xenopus* APC/C. The overall uncertainty is composed of the standard deviation and the 5% calibration uncertainty of the instrument.

(B and C) Histograms showing the mass distributions obtained for human and *Xenopus* APC/C, respectively. All particle orientations were included in the measurement. In spite of the relatively low contrast of the unstained samples employed, as shown in the galleries, typical V shape projections could often be distinguished that yielded masses in the range of the histogram peak. A few visibly smaller particles had masses below 0.5 MDa, whereas others were clearly aggregates of two or more complexes (data not shown). Scale bar, 25 nm.

Furthermore, the view from the back of the APC/C complex clearly reveals the handedness of the structure, by depicting the directionality of the arc lamp domain in all reconstructions.

Molecular Masses and Subunit Stoichiometries of Human and *Xenopus* APC/C

To obtain accurate molecular mass values for APC/C, we analyzed preparations of freeze-dried unstained human and *Xenopus* APC/C by STEM. Values of ~1.4 and ~1.5 MDa (±200 kDa) were measured for human and *Xenopus* APC/C, respectively (Figure 3).

Human APC/C is known to contain 12 subunits, which would represent a mass of ~850 kDa if each subunit was present only once per APC/C particle (reviewed in Herzog and Peters [2005]) (Figure S1 available in the Supplemental Data with this article online). Mass spectrometric analyses of purified human APC/C confirmed the presence of a human ortholog of Swm1/Apc13 in APC/C (Figure S1) that had so far only been detected by immunoblot experiments (Schwickart et al., 2004), but we could not obtain clear evidence for the presence of additional subunits that could contribute to the mass of APC/C (data not shown). Some APC/C subunits may therefore be present in more than one copy per particle.

To test this possibility, we measured the relative stoichiometry of subunits in purified human APC/C. Because the accuracy of methods for such measurements is limited, we employed four different techniques. In one approach, we metabolically labeled proteins in logarithmically proliferating HeLa cells with ^{35}S-methionine or ^{35}S-cysteine, isolated APC/C, quantified the intensity of ^{35}S incorporation per subunit, and normalized the data according to the number of methionine or cysteine residues that are present in different subunits (Figure 4A). In two other approaches, we purified APC/C from unlabeled cells, separated different amounts of protein by SDS-PAGE, stained the subunits either by Sypro-Ruby or by Coomassie blue, and quantified the intensity of the different bands by densitometry (Figures 4B and 4C). In the fourth approach, we extracted APC/C subunits from Coomassie-stained SDS gels, subjected them to quantitative amino acid analyses, and used the resulting data for calculation of stoichiometries (Figure 4D). The eight largest subunits of APC/C could be detected by all four methods, although Cdc27 and Apc4 migrated so closely to each other that their intensities could not be quantified separately. In contrast, the small subunits Doc1, Cdc26, Apc11, and Swm1 could not be reliably detected in all experiments, and we therefore excluded them from our analyses. The analyses of all data sets revealed that the subunits Cdc16, Apc7, and Cdc23 are present in 2- or even in 3-fold higher amounts than the other APC/C subunits. This observation, combined with the finding that human APC/C has a mass of ~1.4 MDa, implies that most of the large

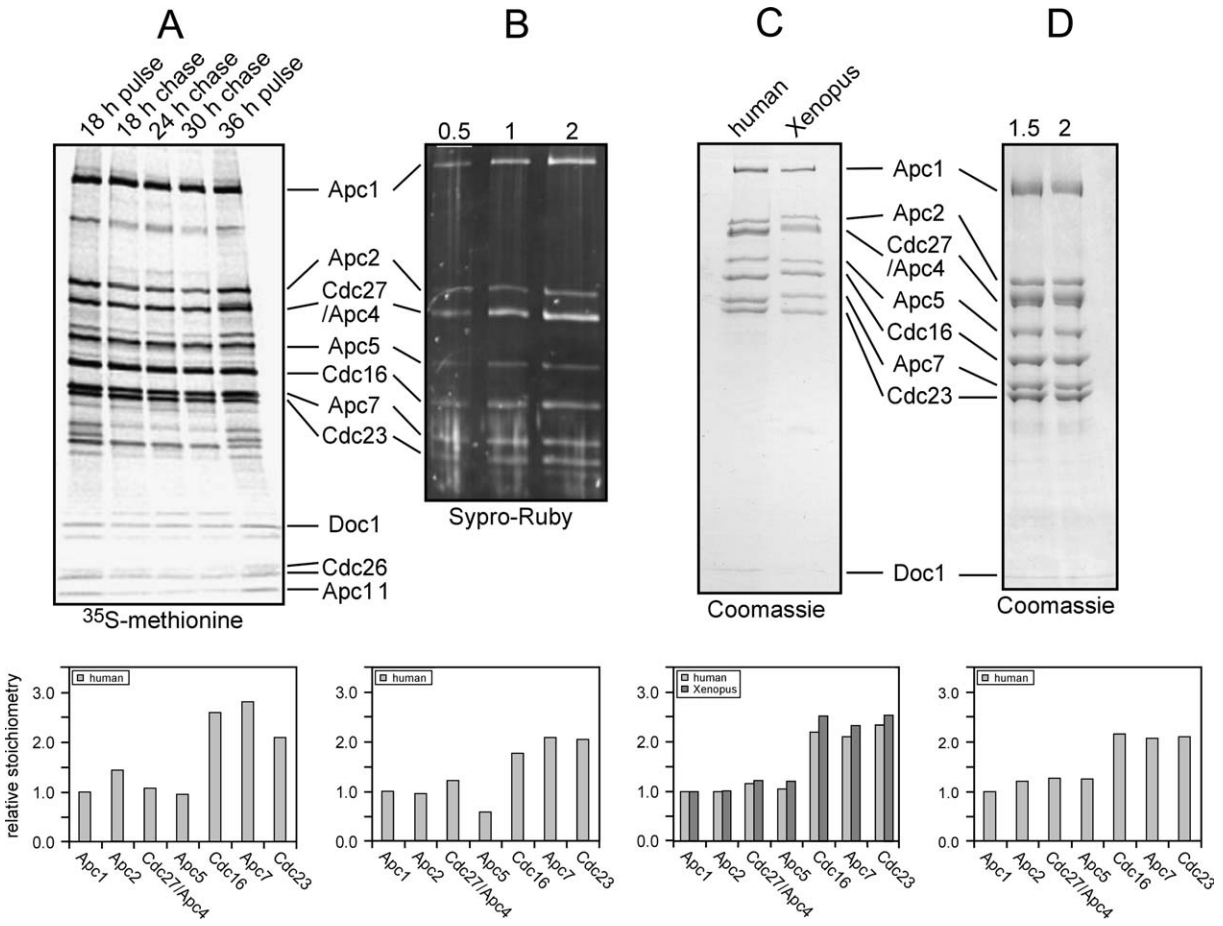

Figure 4. Determination of APC/C Subunit Stoichiometry

(A) Pulse-chase labeling of human APC/C. HeLa cells were pulse labeled with ^{35}S-methionine for 18 hr and subsequently chased for 18, 24, and 30 hr. APC/C was isolated on Cdc27 antibody beads from cell lysates, and proteins were separated by SDS-PAGE and quantified by autoradiography (top). For stoichiometry calculation, the sample from the 24 hr chase was analyzed. Counts per subunit were normalized by the number of methionine residues, and this ratio was set to 1 for Apc1 (bottom).

(B) Sypro-Ruby staining of human APC/C. Increasing amounts (lanes 0.5, 1, and 2) of human APC/C were analyzed by SDS-PAGE and Sypro-Ruby staining (top). The staining intensity per subunit was normalized by the molecular mass of the subunit and set to 1 for Apc1 (bottom).

(C) Coomassie staining of human and *Xenopus* APC/C (top). The subunit stoichiometry was determined as described in (B) (bottom).

(D) Amino acid analysis of human APC/C. Different dilutions of APC/C (lanes 1.5 and 2) were analyzed by SDS-PAGE and Coomassie staining (top), individual subunits were quantified by amino acids analyses, and the resulting data used for determination of stoichiometry (bottom).

subunits of APC/C are present once per particle, whereas there may be two or three copies each of Cdc16, Apc7, and Cdc23 per complex (see Figure S1 for calculations).

Localization of the Coactivator Cdh1 in APC/C^{Cdh1}

The association of Cdh1 with APC/C during exit from mitosis and in the G1 phase leads to APC/C activation, at least in part because the WD40 domain of Cdh1 represents a receptor for the D box of APC/C substrates (Kraft et al., 2005). To identify the Cdh1 binding site, we reconstituted active APC/C^{Cdh1} from purified APC/C and recombinant Cdh1 and analyzed the structure of the resulting complex. We used *Xenopus* APC/C isolated from interphase egg extracts for these experiments because *Xenopus* eggs contain little if any Cdh1 (Kramer et al., 2000), and APC/C purified from these cells has therefore not bound to Cdh1 (in contrast to APC/C samples from logarithmically proliferating HeLa cells that contain substoichiometric amounts of Cdh1; data not shown). In interphase extracts, *Xenopus* APC/C is also not bound to the mitosis-specific coactivator Cdc20 (Kramer et al., 2000), which might bind to the same APC/C site as Cdh1 (Kraft et al., 2005). A comparison between the 3D maps of *Xenopus* interphase APC/C in its "naked" and its Cdh1 bound form should thus reveal the location of the Cdh1 binding site.

Purified *Xenopus* APC/C was incubated with recombinant Cdh1 carrying a His_6-HA tag at its N terminus. After removal of unbound Cdh1, the resulting APC/C^{Cdh1} was analyzed by SDS-PAGE followed by silver staining (Figure 5A) or quantitative immunoblotting, which revealed that Cdh1 associates with 50%–60% of APC/C particles under these conditions (Figure S2). The structure of APC/C^{Cdh1} was analyzed by negative staining cryo-EM and angular reconstitution. Because not all APC/C particles had been loaded with Cdh1, images of APC/C with additional densities were separated

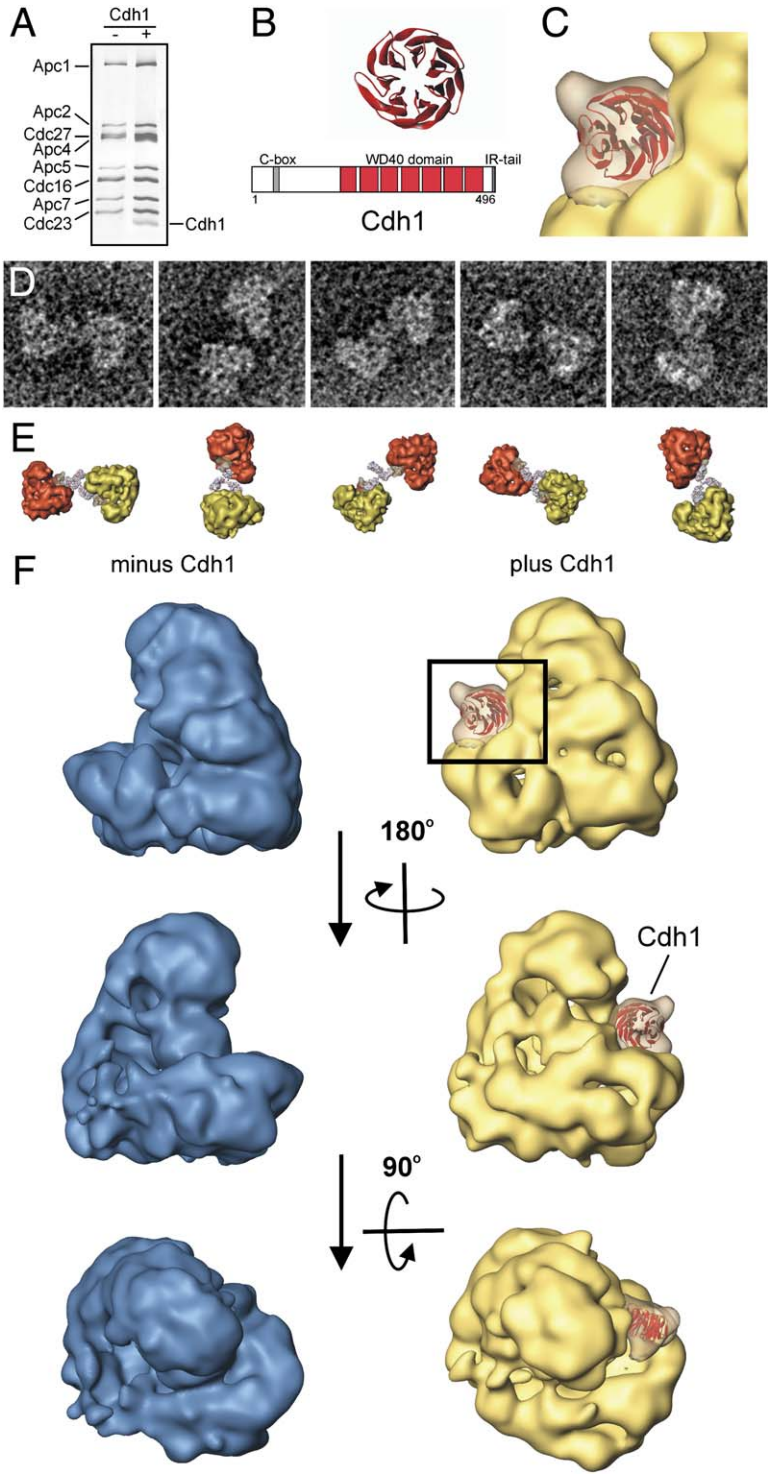

Figure 5. Localization of the Coactivator Cdh1 within the APC/C

(A) APC/C immunopurified from *Xenopus laevis* interphase eggs was loaded in vitro with recombinant human Cdh1. APC/C and APC/C^{Cdh1} were analyzed by SDS-PAGE and silver staining.

(B) Structural domains of Cdh1. The most prominent part of the protein consists of a WD40 repeat that folds into a seven-bladed propeller-like structure as indicated in red (PDB entry: 1GXR).

(C) Close up of the fit of Cdh1's WD40 domain into the *Xenopus* APC/C^{Cdh1} structure.

(D) Antibody labeling of *Xenopus* APC/C^{Cdh1} by an antibody directed against the HA tag on His_6-HA-Cdh1. Characteristic immunocomplexes consisting of two APC/C complexes and an antibody are formed that reveal similar antibody binding sites when compared with the antibody directed against Apc2 (see Figure 6).

(E) Surface views of the APC-antibody complexes shown according to their orientation presented in (D).

(F) The main difference density between *Xenopus* APC/C with and without Cdh1 is located between the arc lamp domain and the platform and also binds to the central density element. The complex is shown from three different orientations as indicated. The extra density in the *Xenopus* APC/C^{Cdh1} structure is shown in semitransparent yellow with a WD40 domain (red) placed into this density.

from images of naked APC/C in the final image processing refinement round based on crosscorrelation alignment with two different sets of references. The resulting 3D model of APC/C^{Cdh1} reveals small differences in several areas compared to that of APC/C without Cdh1, but there is one single location where the APC/C^{Cdh1} model contains a prominent density that is missing in naked APC/C (Figures 2A and 5F). This extra density is located on the right-hand side (front view) of the outer protein wall. The volume and shape of this density are consistent with a 55 kDa WD40 repeat protein (Figure 5B). Docking of a WD40 domain into this density provides an excellent fit (Figures 5C and 5F and Movie S2). However, the precise rotational orientation of the WD40 ring cannot be determined due to low resolution of the model.

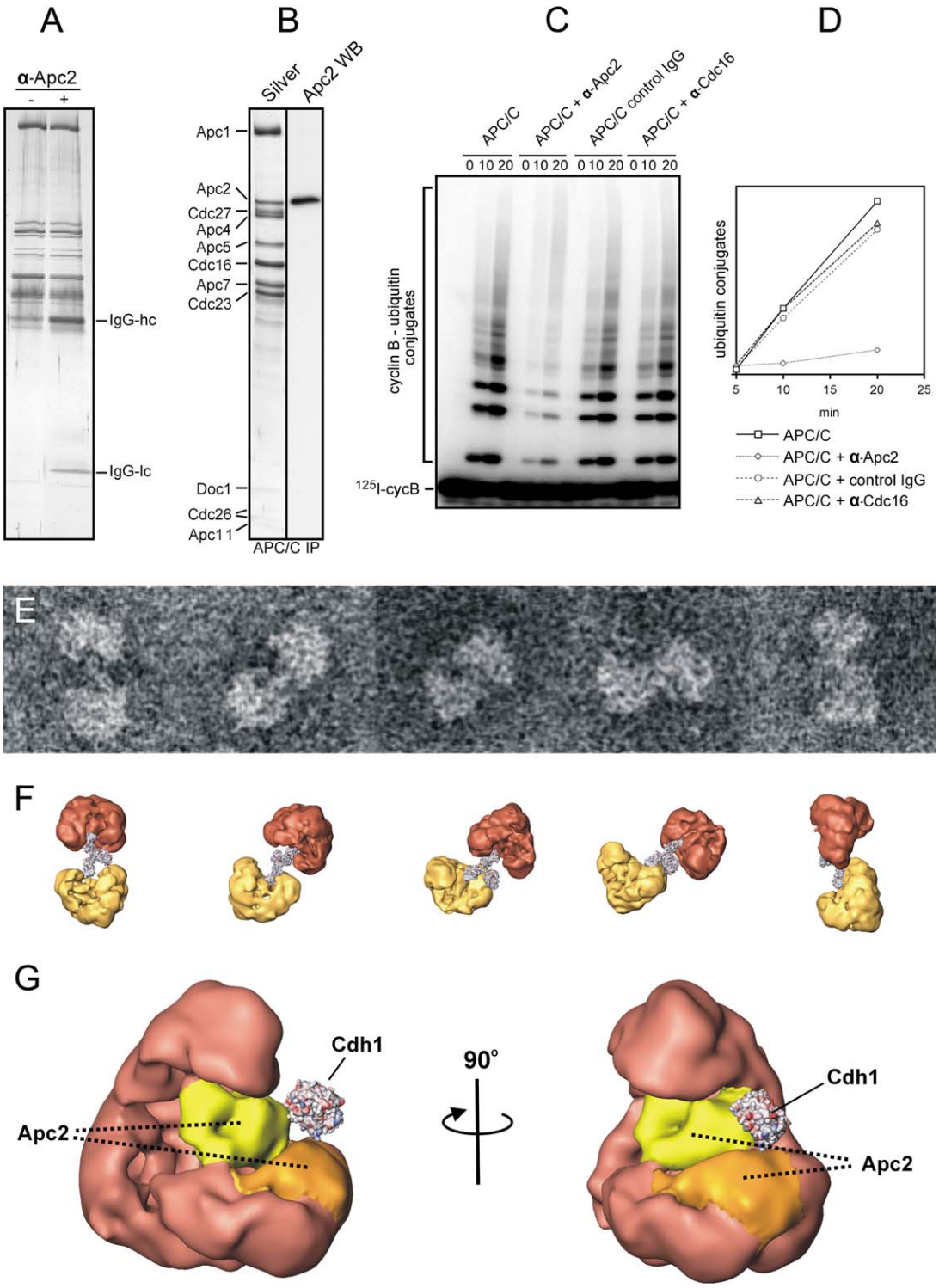

Figure 6. Localization of Apc2 by Antibody Labeling

(A) Stoichiometric binding of the Apc2 antibody to APC/C. Human APC/C was isolated on Cdc27 antibody beads. APC/C peptide eluate was incubated with a monoclonal mouse Apc2 antibody and reisolated by Apc4 antibody beads and subsequent peptide elution. Proteins were detected by SDS-PAGE and silver staining.

(B) Specificity of the Apc2 antibody in Western blot analysis. Immunopurified APC/C was analyzed by SDS-PAGE, silver staining, and Western blotting using a mouse monoclonal Apc2 antibody.

(C) Specific inhibition of APC/C ubiquitination activity by an Apc2 antibody. In vitro ubiquitination activity of human APC/C was assessed in the absence or presence of control IgGs, a polyclonal rabbit Apc2 antibody, or a rabbit Cdc16 antibody by using ^{125}I labeled cyclin B as a substrate. Reactions were stopped at the indicated time points (min) and analyzed by SDS-PAGE and autoradiography.

(D) Quantification of the in vitro ubiquitination assay described in (C).

A smaller density element appears on the left-hand side of the APC/C^{Cdh1} structure (Figure 2A front, and Figure 5F, bottom row), which is too small to accommodate Cdh1. The same region (on the left-hand side) in the *Xenopus* APC/C 3D reconstruction without Cdh1 reveals density that is smeared out, probably due to some local disorder of the APC/C in that region. It is possible that this minor extra density in APC/C^{Cdh1} results from stabilizing this region of the complex upon Cdh1 binding.

To confirm the Cdh1 localization on the right-hand side of APC/C ^{Cdh1}, we labeled *Xenopus* APC/C ^{Cdh1} with antibodies against the HA tag on His_6-HA-Cdh1 (Figures 5D and 5E). In negatively stained preparations, we could see pairs of APC/C particles whose relative position to each other implied that they had been dimerized by simultaneous binding of one HA antibody to two APC/C^{Cdh1} particles, and in some cases, the antibody itself could be seen within these immunocomplexes (Figures 5D and 5E). To localize the antibody binding site on the APC/C surface, we determined the angular orientation of each APC/C within these immunocomplexes. Various orientations of APC/C were found, and this allowed us to narrow down the antibody binding site to the right-hand side of APC/C (Figure 5E). We therefore attribute the additional density found on the right-hand side of the 3D model of APC/C ^{Cdh1} to Cdh1.

Localization of the Cullin Domain of Apc2 in APC/C

The catalytic core of APC/C is formed by the interaction of E2 enzymes with the RING finger subunit Apc11, which in turn binds to the cullin domain of Apc2. To determine the location of the catalytic core, we labeled APC/C with antibodies raised against the cullin domain of Apc2. When human APC/C was incubated with these antibodies, reisolated, and analyzed by SDS-PAGE and silver staining, IgG heavy and light chains could be seen in near-stoichiometric amounts, indicating that the Apc2 antibodies bind efficiently to native APC/C (Figure 6A). In Western blot experiments, the same antibodies only reacted with Apc2, implying that they are specific for Apc2 (Figure 6B). Furthermore, we noticed that some Apc2 antibodies were able to inhibit the ubiquitination activity of the APC/C, whereas antibodies to other subunits such as Cdc27 and Cdc16 did not (Figures 6C and 6D). This confirms the notion that the cullin domain of Apc2 is required for the catalytic activity of APC/C.

In negatively stained preparations, we observed that also Apc2 antibodies were able to dimerize APC/C, and we therefore used the approach described above for His_6-HA-Cdh1 to determine the region of APC/C in which Apc2 is located (Figures 6E and 6F). This procedure unambiguously revealed that the Apc2 antibodies bind to the concave front side of APC/C between the platform and the arc lamp. If one assumes that Apc2 adopts a structure whose overall shape is similar to the shape of the cullin Cul1, whose structure has been determined by crystallography (Zheng et al., 2002), two structural elements on this side of the APC/C 3D map would provide sufficient space for Apc2 (Figure 6G). Interestingly, both are relatively close to the location of Cdh1.

Structural Flexibility of the Arc Lamp Domain

None of the APC/C structures that we determined by angular reconstitution exceeded 24 Å resolution. This limitation is explained by a significant conformational heterogeneity present within the various projection subsets, especially in case of human APC/C. For example, when we analyzed a subset of human APC/C (V shaped) images in detail, we observed a movement of the two main structural domains of APC/C relative to each other; when the platform was aligned in a fixed position, the arc lamp domain was detected in various orientations by local multivariate statistical analysis (Figures 7A–7D). Thus, there seems to be a flexible region connecting the platform and the arc lamp domain. This flexibility creates a relatively high level of projection heterogeneity and consequently limits the attainable resolution.

Similar heterogeneity problems were detected in the case of *Xenopus* APC/C, although to a lower extent, perhaps because in this case, APC/C was purified from synchronized interphase extracts, whereas human APC/C was isolated from a mixed "log phase" population of cells that were in different stages of the cell cycle. Interestingly, when the structures of *Xenopus* APC/C and *Xenopus* APC/C^{Cdh1} are compared, one of the most obvious differences, apart from the presence or absence of the Cdh1 density, is the difference in the relative position of the arc lamp domain and the platform. In *Xenopus* APC/C^{Cdh1}, the position of the arc lamp appears to be rotated by approximately ten degrees compared to the position of this domain in *Xenopus* APC/C without Cdh1 (Figure 7E). This observation suggests that the possibility to adapt different conformations of the platform-arc lamp interface may be of importance for the function or regulation of APC/C.

Discussion

Although APC/C is an essential regulator of mitosis and meiosis in eukaryotes from yeast to men, it is still unknown how this large complex assembles ubiquitin chains on its substrates. It is particularly mysterious why APC/C is composed of so many different subunits and what their functions are. Information about the structure of APC/C will be important for understanding these issues. Here, we report a refined 3D model of vertebrate APC/C in which we have identified the binding site for the APC/C coactivator Cdh1 and have narrowed down the region in which the cullin subunit Apc2 is located and where, therefore, transfer of ubiquitin residues from E2 enzymes to substrates must take place. We also show that APC/C can exist in different conformations, which may have important technical and biological implications.

(E) Immunocomplexes consisting of two human APC/C particles that are bound to an antibody directed against Apc2.
(F) Surface view of the immunocomplexes showing the APC/C in many different orientations.
(G) The Apc2 antibody binds to a region located between the platform and the arc lamp domain, close to the location of Cdh1 in *Xenopus* APC/C. Two potential locations that are large enough to accommodate the cullin domain of Apc2 are colored in yellow and orange.

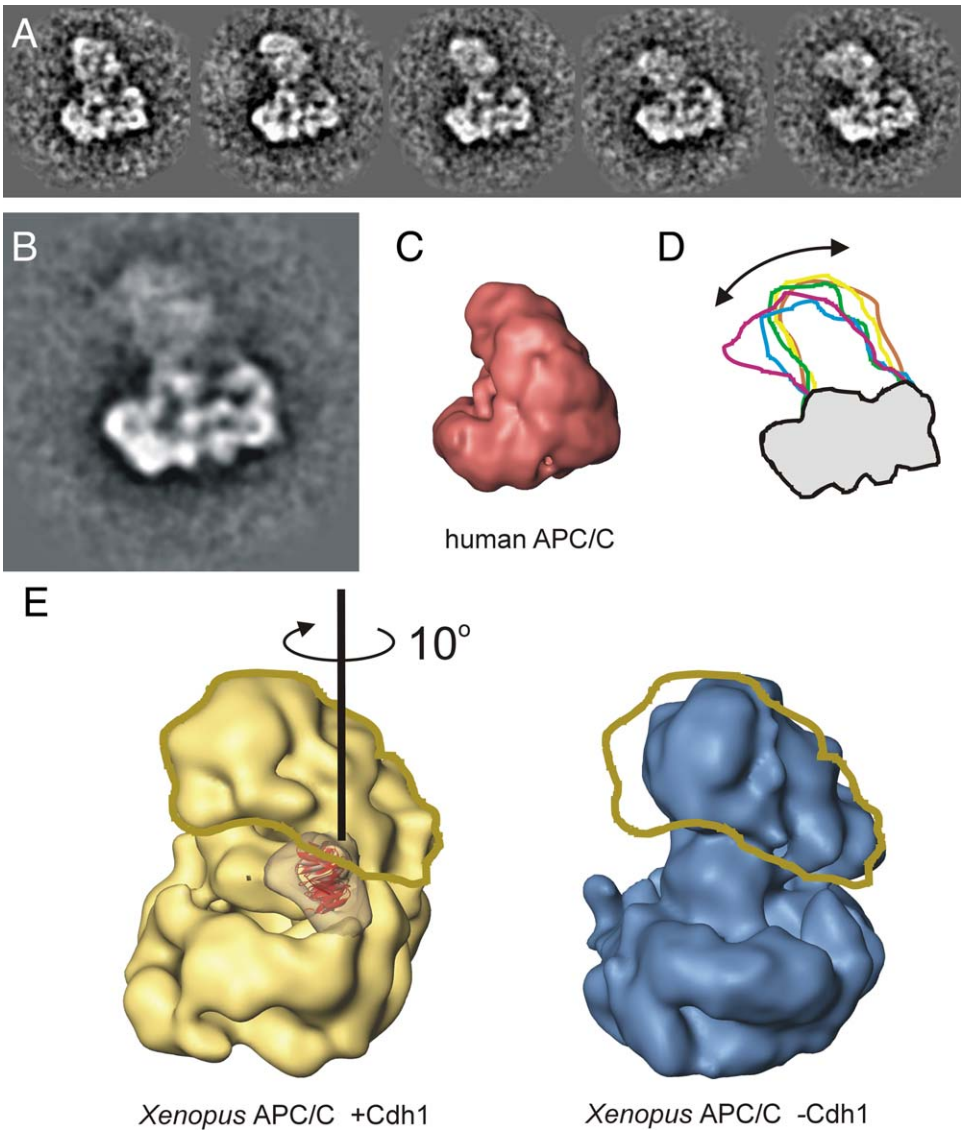

Figure 7. Structural Flexibility of Human and *Xenopus* APC/C

(A) Several class averages of human APC/C are shown in the same projection direction. The bottom part of the images is almost identical, whereas the top part adopts different conformations.

(B) Average of the five class averages shown in (A). The bottom part of the image is well defined, whereas the top density is smeared out due to the different relative orientations of this region and the arc lamp domain.

(C) Corresponding surface view of the class average in (B).

(D) Superposition of contour lines of the five individual class averages shown in (A). The contour lines shown in different colors display the structural flexibility of the arc lamp domain with respect to the gray domain.

(E) Structural flexibility of the arc lamp observed for the *Xenopus* APC/C structure (blue) upon binding to Cdh1 (yellow). The arc lamp domain is rotated by ten degrees upon binding of Cdh1. The same yellow contour line is shown indicating the different rotational orientation of the arc lamp domain.

Where in the APC/C Structure Are Substrates Ubiquitinated?

Our new 3D model has confirmed features that we observed in an earlier model of human APC/C (Gieffers et al., 2001), such as an asymmetric shape and the presence of a large cavity that is surrounded by a protein wall, but our new reconstructions also revealed that APC/C's protein wall does not contain a large opening into the inner cavity. Based on the observation that such an opening could be seen in our earlier 3D model, we discussed the possibility that APC/C's internal cavity could be the site where ubiquitination reactions take place (Gieffers et al., 2001). This remains a possibility because the central cavity is also connected with the outside world through several channels in the new model. However, because our data show that Cdh1 binds to the outside of APC/C and because Cdh1 appears to participate in the recruitment of substrates to the APC/C, it is now more plausible to assume that ubiquitination reactions take place on the outer surface of APC/C. These reactions must occur in close vicinity to the cullin domain of Apc2, which is located on the concave "front"

side of APC/C, because the cullin domain is known to bind to Apc11, which in turn interacts with Ubc4. Interestingly, there is a distance of ~40 Å between the Cdh1 binding site and the candidate locations for the cullin domain of Apc2. It is therefore possible that APC/C's substrate binding domain (Cdh1) is separated from ubiquitin-charged E2 enzymes by a relatively large gap, similar to that observed in other RING finger ubiquitin ligases such as SCF1 and c-Cbl where these gaps span 50 and 60 Å, respectively (Zheng et al., 2002; Zheng et al., 2000).

What Are the Technical Implications of Structural Flexibility in APC/C?

In human APC/C, we detected significant structural flexibility between the platform and the arc lamp domain (Figure 7). This flexibility created serious problems for 3D structure determination because such analyses rely on the assumption that all projection images are derived from structurally identical objects.

Initially, the significant amount of projection heterogeneity made it difficult to determine a correct 3D model of APC/C. A subset of the pseudo symmetrical V shaped views was the most heterogeneous. This set of APC/C projections only differed in the relative orientation of one domain with respect to the other (Figure 7). If this heterogeneity is disregarded during image processing, correct angular orientations with respect to a single 3D structure can no longer be computed. This flexibility also made it very difficult to distinguish between mirror views during Euler angle assignment. If undetected, these views will strongly bias the image analysis, leading to a pseudo symmetrical 3D model. The pseudo symmetrical character is difficult to remove and will persist in subsequent refinement steps. The "refined" 3D structure will even appear to be correct by showing an increase in resolution according to standard criteria. In our case, the initially obtained wrong pseudo symmetrical APC/C model was refined to ~14 Å resolution. Because there is still no general tool available in single particle image analysis to confirm the validity of the reconstruction, it is dangerous to introduce such artifact, especially when working with complexes that are asymmetrical.

However, by careful selection of the views used to compute the first 3D model, we were able to avoid this bias introduced by the dominant V shape images. This resulted in 3D structures that do not suffer from pseudo symmetry problems and fit very well with the independent RCT structure. We are therefore confident that the new 3D models reflect the structures of human and *Xenopus* APC/C with reasonable accuracy.

What Are the Biological Implications of Structural Flexibility in APC/C?

The structural flexibility of the arc lamp domain with respect to the main body observed in human APC/C samples is striking (Figure 7A and Movie S1). However, this phenomenon could simply represent a lack of tight protein-protein interactions. For example, the connection between the platform and the arc lamp domains of APC/C could be less rigid than other parts of the complex, and this property could lead to structural deformations during particle adsorption on the carbon surface. Although we cannot exclude this possibility, there are reasons to believe that the flexibility may be of biological relevance. First, there is good precedence from the analysis of other macromolecular complexes that structural flexibility is functionally important. A famous example is the bacterial ribosome, where structural flexibility in the L7/L12 stalk is thought to be required for elongation factor delivery and GTPase activation (Diaconu et al., 2005). Second, we have observed evidence for flexibility not only in human APC/C but also in the *Xenopus* complex. Third, and most importantly, the binding of Cdh1 to *Xenopus* APC/C correlates with a relative movement between the same two domains, the platform and the arc lamp, whose relative position to each other is also variable in human APC/C.

It is therefore possible that binding of Cdh1 to APC/C induces a conformational change. Such a change could expose sites on APC/C that contribute to substrate binding, or the structural rearrangements could help to position the E2 enzyme and the substrate relative to each other for efficient ubiquitin transfer. It is even possible that APC/C cycles through different conformational states while it is assembling a multiubiquitin chain on a substrate molecule in a processive manner. To test these ideas, an interesting next step will be to analyze if structural changes also occur when APC/C is phosphorylated in mitosis and subsequently binds to its mitosis-specific coactivator Cdc20.

Experimental Procedures

Purification of Human and *Xenopus laevis* APC/C

Human and *Xenopus* APC/C was isolated on Cdc27 antibody cross-linked protein A beads as described (Gieffers et al., 2001; Herzog and Peters, 2005). Briefly, bound protein was washed four times with 50 bead volumes of TBS (20 mM Tris-HCl [pH 7.6], 150 mM NaCl, and 0.5 mM DTT). APC/C was eluted with TBS containing 1 mg/ml Cdc27 peptides for 30 min at 4ºC. Peptides were removed by dialysis against HBS (20 mM HEPES [pH 7.6], 150 mM NaCl, and 0.5 mM DTT) for 6 hr or overnight at 4ºC. Prior to negative staining, APC/C was fixed by incubation with 0.1% paraformaldehyde or glutaraldehyde for 60 min on ice.

Localization of APC/C Subunits

Loading of Recombinant Cdh1 In Vitro

N-terminally His_6-HA-tagged human Cdh1 was expressed in baculovirus-infected Sf9 cells and purified via its His_6-tag (Kraft et al., 2005). Immunopurified *Xenopus* APC/C bound to Cdc27 antibody beads was incubated with 50 ng recombinant Cdh1 per μl beads for 45 min at 4ºC. Beads were washed three times with 50 volumes of TBS and subsequently peptide eluted as described.

Antibody Labeling

Peptide-eluted human APC/C or *Xenopus* APC/C loaded with His_6-HA-Cdh1 was incubated with decreasing amounts of a monoclonal mouse Apc2-30 or HA antibody, respectively, starting at a molar APC/C to IgG ratio of 2:1.

Stoichiometry Measurements

In Vivo Labeling

HeLa cells were grown to 50% confluency in DMEM supplemented with 10% FCS. Cells were washed twice with PBS, pulse labeled by addition of MEM (without methionine or cysteine) supplemented with 2% FCS and 700 μCi ^{35}S-methionine or ^{35}S-cysteine for 18 hr, and subsequently chased for 18, 24, or 30 hr. APC/C was purified on Cdc27 antibody beads from cell lysates at different time points as described (Herzog and Peters, 2005) and analyzed by SDS-PAGE and autoradiography. APC/C subunits appear to have similar half-lives (data not shown), and ^{35}S signals were therefore not

corrected for subunit half-lives. Experiments with ^{35}S-methionine and ^{35}S-cysteine yielded similar results.

Quantitative Protein Staining

Immunoprecipitated human and *Xenopus* APC/C was eluted with antigenic Cdc27 peptide or 100 mM glycine. APC/C eluates were analyzed by SDS-PAGE and Coomassie blue R250 or Sypro-Ruby (Amersham) staining. Staining intensities were measured by the Typhoon Variable Mode Imager (Amersham) and quantified by using the ImageQuant software (Amersham).

Amino Acid Analysis

Purified human APC/C was mixed with SDS to a final concentration of 0.5% and concentrated by ultrafiltration (Vivaspin). APC/C was separated on an SDS-polyacrylamide gel and stained with Coomassie blue R250. Individual APC/C subunits were excised from the gel, proteins subjected to acidic hydrolysis, and amino acids were subsequently quantified by ion-exchange HPLC (Beckman Model 7300). The amino acid analysis was performed by the Protein Chemistry facility of the W.M. Keck Foundation, Yale (http://keck.med.yale.edu/prochem/aaa.htm). The molar ratios of amino acids of the individual subunits were used to calculate APC/C subunit stoichiometry.

STEM Analysis

Samples containing peptide eluted APC/C (5 μl) were adsorbed for 60 s to glow-discharged thin carbon films that spanned a thick fenestrated carbon layer covering 200 mesh/inch, gold-plated copper grids. The grids were then blotted, washed on five drops of either 100 or 500 mM ammonium acetate prepared with quartz double-distilled water, plunge frozen, and freeze dried at −80ºC and 5×10^{-8} Torr overnight in the microscope. Tobacco mosaic virus (TMV; kindly supplied by Dr. R. Diaz-Avalos, Institute of Molecular Biophysics, Florida State University) served as a mass standard.

A Vacuum Generators STEM HB-5 interfaced to a modular computer system (TVIPS GmbH, Gauting, Germany) was employed. Series of 512 × 512 pixel, dark-field images were recorded from the unstained samples at an accelerating voltage of 80 kV and a nominal magnification of 200,000×. The recording dose ranged from 248 to 620 electrons/nm^2. Further, repetitive low dose scans were made of some grid regions to assess beam-induced mass loss as outlined in Müller et al. (1992). The digital images were evaluated by using the program package IMPSYS (Müller et al., 1992). Accordingly, the projections were selected in circular boxes, and the total scattering of each region was calculated. The background scattering of the carbon support film was then subtracted and the mass calculated. Finally, the results were corrected for the beam-induced mass loss, which varied between 2.8% and 7.3% depending on the dose employed, scaled according to the mass standard, displayed in histograms, and described by Gauss curves.

EM of APC/C

APC/C samples were prepared by the double carbon layer cryo-negative stain procedure (Golas et al., 2003). Briefly, APC/C particles were embedded in a mixture of buffer, glycerol, and uranyl formate while being sandwiched between two carbon films. After final blotting of the stain solution, the grids were left for ~1 min at RT prior to freezing and storing them in liquid nitrogen. Images were taken on a Philips CM200 FEG microscope either at 161,000× (human APC/C) or 91,000× magnification (*Xenopus* APC/C) on a TVIPS 4kx4k slow scan CCD camera in 2×-fold binning mode. Additional data sets were recorded on film confirming the computed 3D structures presented in this manuscript (data not shown). Prior to computational analysis, the human APC/C images were coarsened by a factor of two, leading to a pixel size of 3.81 Å/pixel, whereas the *Xenopus* APC/C data had a pixel size of 3.32 Å/pixel (not coarsened). Because images of APC/C obtained by cryo-negative stain appeared larger than STEM images (Boisset et al., 1993), we have calibrated the cryo-negative stain images by using the more accurate STEM data. The calibrated pixel sizes of the cryo-negative stain data are ~13% smaller than stated above. Using the calibrated pixel size, the molecular mass enclosed by the boundaries of the APC/C structures presented as surface representations fits very well to the experimental mass determined by the STEM analysis. During model building, we noticed that the dimensions of both human and *Xenopus* APC/C are larger than those we had reported previously (Gieffers et al., 2001) and realized that this difference is due to an error in the pixel size that was assumed for the previous model calculation. The corrected (calibrated) dimensions of vertebrate APC/C are ~226 Å from top to bottom and ~200 × 180 Å for the size of the platform (Figure 2A).

A total of 30,308 molecular images were selected in the case of human APC/C. The number of particles in the two *Xenopus* datasets was 7395 for *Xenopus* plus Cdh1 and 5533 for *Xenopus* minus Cdh1. The raw images were corrected for the contrast transfer function by phase flipping as described (Sander et al., 2003a). Standard image processing procedures, including alignment (Sander et al., 2003b), multivariate statistical analysis (van Heel, 1984), classification, and angular reconstitution (van Heel, 1987), were used as implemented in the Imagic-5 image processing software (van Heel et al., 1996). The final resolution of the 3D maps was ~24 Å (26 Å) for both *Xenopus* APC/C maps and 25 Å (28 Å) for the human APC/C map as determined by the Fourier-shell-correlation function (Harauz and van Heel, 1986) using the 5 sigma criterion (or the FSC 0.5 criteria).

The RCT reconstruction (Radermacher, 1988) was determined from 2039 tilted image pairs of the *Xenopus* sample (without Cdh1). Images have been recorded on the CCD camera to obtain maximum image quality for better performance during image alignment and classification (Sander et al., 2005).

Supplemental Data

Supplemental Data include Supplemental Experimental Procedures, Supplemental References, two figures, and two movies and can be found with this article online at http://www.molecule.org/cgi/content/full/20/6/867/DC1/.

Acknowledgments

We are grateful to Karl Mechtler and Mathias Madalinski for peptide synthesis and thank Philippe Ringler and Françoise Erne-Brand for carrying out the STEM microscopy. We also thank Jochen Deckert and Reinhard Lührmann for support. Research in the laboratory of A.E. was supported by Swiss National Foundation grant number NF 3100-059415 and the Maurice E. Müller Foundation of Switzerland. Research in the laboratory of J.-M.P. was supported by Boehringer Ingelheim, the Sixth Framework Programme of the European Union via the Integrated Project Mitocheck, the Austrian Science Fund, and the European Molecular Biology Organization (EMBO). Research in the laboratory of H.S. was supported by grants from the Federal Ministry of Education and Research, Germany (031U215B and 0311899) and the Sixth Framework Programme of the European Union via the Integrated Project 3DRepertoire.

Received: August 5, 2005
Revised: October 21, 2005
Accepted: November 8, 2005
Published: December 21, 2005

References

Au, S.W., Leng, X., Harper, J.W., and Barford, D. (2002). Implications for the ubiquitination reaction of the anaphase-promoting complex from the crystal structure of the Doc1/Apc10 subunit. J. Mol. Biol. *316*, 955–968.

Boisset, N., Radermacher, M., Grassucci, R., Taveau, J.C., Liu, W., Lamy, J., Frank, J., and Lamy, J.N. (1993). Three-dimensional immunoelectron microscopy of scorpion hemocyanin labeled with a monoclonal Fab fragment. J. Struct. Biol. *111*, 234–244.

Burton, J.L., Tsakraklides, V., and Solomon, M.J. (2005). Assembly of an APC-Cdh1-substrate complex is stimulated by engagement of a destruction box. Mol. Cell *18*, 533–542.

Diaconu, M., Kothe, U., Schlunzen, F., Fischer, N., Harms, J.M., Tonevitsky, A.G., Stark, H., Rodnina, M.V., and Wahl, M.C. (2005). Structural basis for the function of the ribosomal L7/12 stalk in factor binding and GTPase activation. Cell *121*, 991–1004.

Gieffers, C., Dube, P., Harris, J.R., Stark, H., and Peters, J.M. (2001). Three-dimensional structure of the anaphase-promoting complex. Mol. Cell *7*, 907–913.

Gmachl, M., Gieffers, C., Podtelejnikov, A.V., Mann, M., and Peters, J.M. (2000). The RING-H2 finger protein APC11 and the E2 enzyme UBC4 are sufficient to ubiquitinate substrates of the anaphase-promoting complex. Proc. Natl. Acad. Sci. USA *97*, 8973–8978.

Golas, M.M., Sander, B., Will, C.L., Luhrmann, R., and Stark, H. (2003). Molecular architecture of the multiprotein splicing factor SF3b. Science *300*, 980–984.

Harauz, G., and van Heel, M. (1986). Exact filters for general geometry three-dimensional reconstruction. Optik *73*, 146–156.

Harper, J.W., Burton, J.L., and Solomon, M.J. (2002). The anaphase-promoting complex: it's not just for mitosis any more. Genes Dev. *16*, 2179–2206.

Herzog, F., and Peters, J.M. (2005). Large scale purification of the vertebrate anaphase-promoting complex/cyclosome. Methods Enzymol. *398*, 175–195.

Kraft, C., Vodermaier, H.C., Maurer-Stroh, S., Eisenhaber, F., and Peters, J.M. (2005). The WD40 propeller domain of Cdh1 functions as a destruction box receptor for APC/C substrates. Mol. Cell *18*, 543–553.

Kramer, E.R., Scheuringer, N., Podtelejnikov, A.V., Mann, M., and Peters, J.M. (2000). Mitotic regulation of the APC activator proteins CDC20 and CDH1. Mol. Biol. Cell *11*, 1555–1569.

Leverson, J.D., Joazeiro, C.A., Page, A.M., Huang, H., Hieter, P., and Hunter, T. (2000). The APC11 RING-H2 finger mediates E2-dependent ubiquitination. Mol. Biol. Cell *11*, 2315–2325.

Lorick, K.L., Jensen, J.P., Fang, S., Ong, A.M., Hatakeyama, S., and Weissman, A.M. (1999). RING fingers mediate ubiquitin-conjugating enzyme (E2)-dependent ubiquitination. Proc. Natl. Acad. Sci. USA *96*, 11364–11369.

Müller, S.A., Goldie, K.N., Bürki, R., Häring, R., and Engel, A. (1992). Factors influencing the precision of quantitative scanning transmission electron microscopy. Ultramicroscopy *46*, 317–334.

Passmore, L.A., and Barford, D. (2004). Getting into position: the catalytic mechanisms of protein ubiquitylation. Biochem. J. *379*, 513–525.

Passmore, L.A., Booth, C.R., Vénien-Bryan, C., Ludtke, S.J., Fioretto, C., Johnson, L.N., Chiu, W., and Barford, D. (2005). Structural analysis of the anaphase-promoting complex reveals multiple active sites and insights into polyubiquitylation. Mol. Cell *20*, this issue, 855–866.

Peters, J.M. (2002). The anaphase-promoting complex: proteolysis in mitosis and beyond. Mol. Cell *9*, 931–943.

Petroski, M.D., and Deshaies, R.J. (2005). Function and regulation of cullin-RING ubiquitin ligases. Nat. Rev. Mol. Cell Biol. *6*, 9–20.

Radermacher, M. (1988). Three-dimensional reconstruction of single particles from random and nonrandom tilt series. J. Electron Microsc. Tech. *9*, 359–394.

Radermacher, M., Wagenknecht, T., Verschoor, A., and Frank, J. (1987). Three-dimensional reconstruction from a single-exposure, random conical tilt series applied to the 50S ribosomal subunit of Escherichia coli. J. Microsc. *146*, 113–136.

Sander, B., Golas, M.M., and Stark, H. (2003a). Automatic CTF correction for single particles based upon multivariate statistical analysis of individual power spectra. J. Struct. Biol. *142*, 392–401.

Sander, B., Golas, M.M., and Stark, H. (2003b). Corrim-based alignment for improved speed in single-particle image processing. J. Struct. Biol. *143*, 219–228.

Sander, B., Golas, M.M., and Stark, H. (2005). Advantages of CCD detectors for de novo three-dimensional structure determination in single-particle electron microscopy. J. Struct. Biol. *151*, 92–105.

Schwickart, M., Havlis, J., Habermann, B., Bogdanova, A., Camasses, A., Oelschlaegel, T., Shevchenko, A., and Zachariae, W. (2004). Swm1/Apc13 is an evolutionarily conserved subunit of the anaphase-promoting complex stabilizing the association of Cdc16 and Cdc27. Mol. Cell. Biol. *24*, 3562–3576.

Tang, Z., Li, B., Bharadwaj, R., Zhu, H., Ozkan, E., Hakala, K., Deisenhofer, J., and Yu, H. (2001). APC2 Cullin protein and APC11 RING protein comprise the minimal ubiquitin ligase module of the anaphase-promoting complex. Mol. Biol. Cell *12*, 3839–3851.

van Heel, M. (1984). Multivariate statistical classification of noisy images (randomly oriented biological macromolecules). Ultramicroscopy *13*, 165–183.

van Heel, M. (1987). Angular reconstitution: a posteriori assignment of projection directions for 3D reconstruction. Ultramicroscopy *21*, 95–100.

van Heel, M., Harauz, G., and Orlova, E.V. (1996). A new generation of the IMAGIC image processing system. J. Struct. Biol. *116*, 17–24.

Vodermaier, H.C., Gieffers, C., Maurer-Stroh, S., Eisenhaber, F., and Peters, J.M. (2003). TPR subunits of the anaphase-promoting complex mediate binding to the activator protein CDH1. Curr. Biol. *13*, 1459–1468.

Wendt, K.S., Vodermaier, H.C., Jacob, U., Gieffers, C., Gmachl, M., Peters, J.M., Huber, R., and Sondermann, P. (2001). Crystal structure of the APC10/DOC1 subunit of the human anaphase-promoting complex. Nat. Struct. Biol. *8*, 784–788.

Yu, H., Peters, J.M., King, R.W., Page, A.M., Hieter, P., and Kirschner, M.W. (1998). Identification of a cullin homology region in a subunit of the anaphase-promoting complex. Science *279*, 1219–1222.

Zachariae, W., Shevchenko, A., Andrews, P.D., Ciosk, R., Galova, M., Stark, M.J., Mann, M., and Nasmyth, K. (1998b). Mass spectrometric analysis of the anaphase-promoting complex from yeast: identification of a subunit related to cullins. Science *279*, 1216–1219.

Zheng, N., Wang, P., Jeffrey, P.D., and Pavletich, N.P. (2000). Structure of a c-Cbl-UbcH7 complex: RING domain function in ubiquitin-protein ligases. Cell *102*, 533–539.

Zheng, N., Schulman, B.A., Song, L., Miller, J.J., Jeffrey, P.D., Wang, P., Chu, C., Koepp, D.M., Elledge, S.J., Pagano, M., et al. (2002). Structure of the Cul1-Rbx1-Skp1-F boxSkp2 SCF ubiquitin ligase complex. Nature *416*, 703–709.

Accession Numbers

The structural coordinates have been deposited in the IIMS Database at EMBL EBI. The structure of human APC/C can be accessed under the code EMD-1139. The *Xenopus* APC/C with and without Cdh1 bound can be accessed under EMD-1142 and EMD-1140, respectively.